

Dalton Transactions

Accepted Manuscript

This article can be cited before page numbers have been issued, to do this please use: A. Hens, P. Mondal and K. K. Rajak, *Dalton Trans.*, 2013, DOI: 10.1039/C3DT51571K.



This is an *Accepted Manuscript*, which has been through the RSC Publishing peer review process and has been accepted for publication.

Accepted Manuscripts are published online shortly after acceptance, which is prior to technical editing, formatting and proof reading. This free service from RSC Publishing allows authors to make their results available to the community, in citable form, before publication of the edited article. This *Accepted Manuscript* will be replaced by the edited and formatted *Advance Article* as soon as this is available.

To cite this manuscript please use its permanent Digital Object Identifier (DOI®), which is identical for all formats of publication.

More information about *Accepted Manuscripts* can be found in the [Information for Authors](#).

Please note that technical editing may introduce minor changes to the text and/or graphics contained in the manuscript submitted by the author(s) which may alter content, and that the standard [Terms & Conditions](#) and the [ethical guidelines](#) that apply to the journal are still applicable. In no event shall the RSC be held responsible for any errors or omissions in these *Accepted Manuscript* manuscripts or any consequences arising from the use of any information contained in them.

Dalton Trans. (Revised)

Manuscript ID: DT-ART-06-2013-051571.R1

July, 2013

Synthesis, structure and spectral properties of *O*, *N*, *N* coordinating ligands and their neutral Zn(II) complexes: a combined experimental and theoretical study[†]

Amar Hens, Pallab Mondal, and Kajal Krishna Rajak*

Abstract

The mononuclear Zn(II) complexes of general formula $[Zn(L)_2]$ have been synthesized in good yields by reacting $Zn(OAc)_2$ with HL in ratio of 1:2 in methanol solvent. Here L is the deprotonated form of 6-[(quinolin-8-ylamino)methylene]cyclohexa-2,4-dienone (HL^1), 4-chloro-6-[(quinolin-8-ylamino)methylene]cyclohexa-2,4-dienone (HL^2), 4-methyl-6-[(quinolin-8-ylamino)methylene]cyclohexa-2,4-dienone (HL^3), 2,4-dimethyl-6-[(quinolin-8-ylamino)methylene]cyclohexa-2,4-dienone (HL^4), 2-methoxy-6-[(quinolin-8-ylamino)methylene]cyclohexa-2,4-dienone (HL^5). The electronic structure and photophysical properties of the ligands were calculated by DFT and TDDFT method. The X-ray structure of one complex has been reported. The ligands have strong binding ability $[(0.75-15.37) \times 10^4]$ and ratiometric response to Zn^{2+} ions. Addition of Zn^{2+} ions to the ligands in THF solution a sharp color change is observed visually as well as there occurs a significant enhancement of the fluorescence intensity and the quantum yield for this series. Introduction of other metal ions having biological and environmental effect either keeps unaltered or quenches emission intensity. However we observed the sensing property of the ligands strongly depends on the substituents at the ortho position of the phenol group. The DFT calculation reveals that ICT process take place from salicylaldehyde (donor moiety) to quinoline (acceptor moiety) which is responsible for enhancement of fluorescence intensity of ligands after complexation.

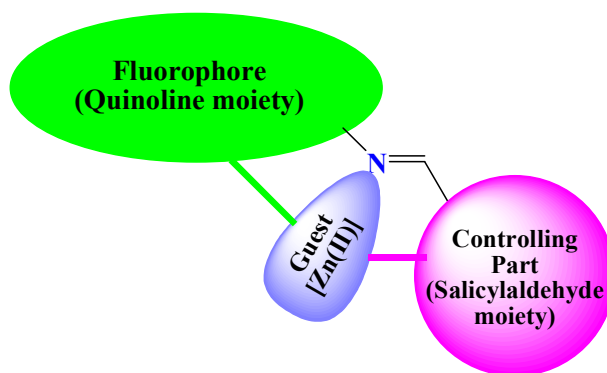
Introduction

The research on electroluminescent materials has received a great deal of attention for decades because of their potential application in the fabrication of organic light emitting diodes (OLED).¹ A variety of fluorescent-sensing approaches have been extensively investigated pertaining to the signaling mechanisms of internal charge transfer² (ICT), photoinduced electron transfer/energy transfer³ (PET), metal-ligand charge transfer⁴ (MLCT), excimer/exciple formation as well as the excited state intramolecular/intermolecular proton transfer⁵ (ESIPT).

Zn(II) ion is spectroscopically as well as magnetically silent due to its $3d^{10}$ electronic configuration. However it can modulate the ligand luminescence properties by means of chelation enhanced fluorescence's (CHEF).⁶⁻¹⁸ The generated CHEF effect is regulated by photoinduced electron transfer (PET) mechanism. In this context the Schiff base complexes of Zn(II) ion are particularly interesting due to their potential photochromic applications.¹⁹⁻²²

In the free Schiff base ligands the nitrogen lone pair electrons at the α position of the fluorophore are induced to the π system of the fluorophores resulting the quenching of their fluorescence. However in the complex the donation of the $-C=N-$ nitrogen lone pair to the metal center enhances the fluorescence intensity through CHEF mechanism.

In the present work we report the successful synthesis of mononuclear Zn(II) complexes containing *O, N, N* coordinating ligands derived from 8-aminoquinoline and salicylaldehyde and its derivatives. The X-ray structure of a complex is reported as a representative case. Here we describe the spectral properties of the synthesized ligands as well as their neutral Zn(II) complexes. The sensing properties of such compounds are governed by the close environment about the metal ion and the small change in the ligand architecture can strongly influence such properties, as in Scheme 1. These demands further investigation of coordination chemistry of zinc(II) incorporating Schiff base ligands having *O, N, N* coordinating sites to understand how a ligand environment modulate their spectroscopic properties.



Scheme 1

Here, we also present a full density functional theory (DFT) and time-dependent density functional theory (TDDFT) investigation to get better insight into the geometry, electronic structure, and optical properties of these systems. Geometry optimization of the singlet ground-state was carried out by means of DFT calculations. TDDFT calculations of several singlet states have been performed for better understanding of the electronic origin of the absorption and emission spectra.

Experimental section

Materials

All the starting chemicals were analytically pure and used without further purification.

Caution! *Perchlorate salts are highly explosive, and should be handled with care and in small amounts.*

Physical Measurements

UV–Vis spectra were recorded on a Perkin–Elmer LAMBDA 25 spectrophotometer. IR spectra were obtained with a Perkin–Elmer L-0100 spectrophotometer. ^1H spectra were measured on Bruker FT 300 MHz spectrometer. The atom-numbering scheme used for ^1H is same as that used in the crystallography. Elemental analyses (C, H, N) were performed on Perkin–Elmer 2400 series II analyzer. The emission data were collected on a Perkin–Elmer LS 55 fluorescence spectrometer.

$$\Phi_r = \Phi_{\text{std}} \frac{A_{\text{std}}}{A_r} \frac{I_r}{I_{\text{std}}} \frac{\eta_r^2}{\eta_{\text{std}}^2} \quad (1)$$

For all luminescence measurements excitation and emission slit width of 5 nm was used. Quantum yields of the complexes were determined in freeze-pump-thaw-degassed solutions of the complexes by a relative method using quinine sulfate in the same solvent as the standard.²³ The quantum yields were calculated using eq 1,²⁴ where Φ_r and Φ_{std} are the quantum yields of unknown and standard samples [$\Phi_{std} = 0.54$ (at 298 K) in THF at $\lambda_{ex} = 460$ nm], A_r and A_{std} (<0.1) are the solution absorbance at the excitation wavelength (λ_{ex}), I_r and I_{std} are the integrated emission intensities, and η_r and η_{std} are the refractive indices of the solvent. Experimental errors in the reported luminescence quantum yields were about 10%.

Computational Details

Among the five ligands (HL¹ to HL⁵), DFT calculation were carried out for two cases (HL¹ and HL²) only. The geometrical structures in their singlet ground state (S_0) and excited state (S_1) were optimized by the DFT²⁵ and time-dependent DFT (TDDFT)²⁶ method with B3LYP exchange correlation functional²⁷ approach associated with the conductor-like polarizable continuum model (CPCM).²⁸

To calculate the stability of the keto tautomeric form over the enol form for the ligands (HL) in ground S_0 state we perform the potential energy scan according to the “distinguished coordinate approach”²⁹ i.e. by specifying a reaction coordinate (in the present case it is the coordinate for translocation of the proton from N_{donor} to $O_{acceptor}$, i.e. elongation of the $N_{donor}-H$ bond axis) along which energy change is observed. For the ground S_0 state all of the other degrees of freedom are relaxed without imposing any symmetry constraints.

On the basis of the optimized ground (S_0) and excited state (S_1) geometry structures of the ligands, the absorption and emission spectral properties in tetrahydrofuran (THF) media were calculated by time-dependent density functional theory (TDDFT) approach associated with the conductor-like polarizable continuum model (CPCM). We computed the lowest 20 singlet – singlet transition both in ground state (S_0) and excited state (S_1) and results of the TDDFT calculations. Due to the presence of electronic correlation in the TDDFT (B3LYP) method it can yield more accurate electronic excitation energies.

DFT calculations were done for two complexes (**2** and **4**). The geometry of the complexes in their ground S_0 state was optimized in solution phase. But we are unable to optimize their singlet excited state (S_1) geometry. For the complexes we also calculated 60 singlet – singlet transition using their ground S_0 state geometry by the same procedure as in ligands.

The effective core potential (ECP) approximation of Hay and Wadt was used for describing the ($1s^22s^22p^6$) core electron for zinc whereas the associated “double- ξ ” quality basis set LANL2DZ was used for the valence shell.³⁰ For H atoms we used 6-31(g) basis set and for C, N and O atoms we employed 6–31+g and for Cl atoms we employed 6-31+g(d,p) as basis set for the optimization of both the ground state and the excited state geometries. The calculated electronic density plots for frontier molecular orbitals were prepared by using the GaussView 5.0 software. All the calculations were performed with the Gaussian 09W software package.³¹ GaussSum 2.1 program³² was used to calculate the molecular orbital contributions from groups or atoms.

Crystallographic Studies

The single crystal suitable for X-ray crystallographic analysis of the complex $[\text{Zn}(\text{L}^4)_2]\cdot\text{CH}_3\text{OH}, 4\cdot\text{CH}_3\text{OH}$ was obtained by slow evaporation of methanolic solution of **4**. The X-ray intensity data were collected on Bruker AXS SMART APEX CCD diffractometer (Mo K_α , $\lambda = 0.71073 \text{ \AA}$) at 293 K. The detector was placed at a distance 6.03 cm from the crystal. Total 606 frames were collected with a scan width of 0.3° in different settings of φ . The data were reduced in SAINTPLUS³³ and empirical absorption correction was applied using the SADABS package.³³ Metal atom was located by Patterson Method and the rest of the non-hydrogen atoms were emerged from successive Fourier synthesis. The structure was refined by full matrix least-square procedure on F^2 . All non-hydrogen atoms were refined anisotropically. All calculations were performed using the SHELXTL V 6.14 program package.³⁴ Molecular structure plots were drawn using the Oak Ridge thermal ellipsoid plot (ORTEP).³⁵ Relevant crystal data is given in Table 1.

Table 1 Crystal Data and Structure Refinement Parameters for 4.CH₃OH

	4.CH ₃ OH
Formula	C ₃₇ H ₃₄ N ₄ O ₃ Zn
M_r	648.05
Crystal system	Triclinic
Space group	<i>P</i> -1
$a / \text{Å}$	11.806(5)
$b / \text{Å}$	12.117(5)
$c / \text{Å}$	12.312(5)
$\alpha / ^\circ$	85.883(5)
$\beta / ^\circ$	62.824(5)
$\gamma / ^\circ$	87.652(5)
$V / \text{Å}^3$	1562.7(11)
Z	2
$D_{\text{calcd}} / \text{mg m}^{-3}$	1.371
μ / mm^{-1}	0.830
$\theta / ^\circ$	1.69 – 27.78
T / K	293(2)
Reflns collected	7281
$R1, ^a wR2^b [I > 2\sigma(I)]$	0.0500, 0.1346
GOF on F^2	1.048

$$^a R1 = \frac{\sum ||F_o| - |F_c||}{\sum |F_o|}$$

$$^b wR2 = [\sum [w(F_o^2 - F_c^2)^2] / \sum [w(F_o^2)^2]]^{1/2}$$

Synthesis of ligands

The ligands were prepared by the same general method. Details are given here for a representative case (HL¹).

HL¹. To a methanolic solution (20 mL) of 2-Hydroxy-benzaldehyde (245 mg, 2 mmol) and 8-aminoquinoline (288 mg, 2 mmol) in presence of 3-4 drops of acetic acid was refluxed in water bath for 2 h. After cooling to room temperature, the solvent was removed under reduced pressure. The crude mass was subjected to column

chromatography on a silica gel column (60-120 mesh). A red band was eluted using 5% ethylacetate in hexane solution. A red colored solid was obtained after removal of solvent under reduced pressure to afford the desired ligand (HL¹). Yield: 406 mg (82%). Elemental Anal. Calcd. for C₁₆H₁₂N₂O: C, 77.04; H, 4.87; N, 11.28. Found: C, 77.12; H, 4.92; N, 11.36. ¹H NMR {300 MHz, CDCl₃, δ (ppm), *J* (Hz)}: 8.93 (H1, d, *J* = 5.9), 8.08 (H10, s), 7.51–6.7 (9H, ArH), 3.51 (NH, bs).

HL². Yield: 435 mg (77%). Elemental Anal. Calcd. for C₁₆H₁₁ClN₂O: C, 67.90; H, 3.92; N, 9.91. Found: C, 68.18; H, 4.06; N, 10.06. ¹H NMR {300 MHz, CDCl₃, δ (ppm), *J* (Hz)}: 8.99 (H1, d, *J* = 5.7), 8.19 (H10, s) 7.74–7.26 (8H, ArH), 3.51 (NH, bs).

HL³. Yield: 424 mg (81%). Elemental Anal. Calcd. for C₁₇H₁₄N₂O: C, 77.84; H, 5.38; N, 10.16. Found: C, 78.12; H, 5.44; N, 10.91. ¹H NMR {300 MHz, CDCl₃ δ (ppm), *J* (Hz)}: 8.77 (H1, d, *J* = 5.8), 8.09 (H10, s) 7.40–6.04 (8H, ArH), 3.49 (NH, bs) 2.27 (CH₃, s).

HL⁴. Yield: 474 mg (86%). Elemental Anal. Calcd. for C₁₈H₁₆N₂O: C, 78.24; H, 5.84; N, 10.14. Found: C, 78.67; H, 5.97; N, 10.28. ¹H NMR {300 MHz, CDCl₃ δ (ppm), *J* (Hz)}: 8.99 (H1, d, *J* = 5.7), 8.16 (H10, s) 7.69–6.91 (7H, ArH), 4.98 (NH, s) 2.33 (CH₃, s), 2.30 (CH₃, s).

HL⁵. Yield: 444 mg (80%). Elemental Anal. Calcd. for C₁₇H₁₄N₂O₂: C, 73.37; H, 5.07; N, 10.07. Found: C, 73.71; H, 5.15; N, 10.29. ¹H NMR {300 MHz, CDCl₃, δ (ppm), *J* (Hz)}: 8.95 (H1, d, *J* = 5.8), 8.10 (H10, s) 7.53–6.85 (8H, ArH), 3.49 (NH, s) 3.95 (OCH₃, s).

Synthesis of complexes

The complexes were synthesized by the same general procedure. Details are given here for a representative case [Zn(L¹)₂], **1**.

[Zn(L¹)₂], 1. To a solution of Zinc(II) acetate dihydrate (34 mg, 0.15 mmol) in methanol (20 mL) was added HL¹ (76 mg, 0.30 mmol), stirred for 2 h. The resulting dark orange colored solution on slow evaporation yielded dark orange crude product. Yield: 74 mg (88%). Elemental Anal. Calcd. for C₃₂H₂₂N₄O₂Zn: C, 68.64; H, 3.96; N, 10.01. Found: C, 68.71; H, 4.01; N, 10.07. IR (KBr, cm⁻¹): ν(C=N) 1641; ν(C–O_{phenoxo}) 1249. ¹H NMR {300 MHz, DMSO–d₆, δ (ppm), *J* (Hz)}: 8.97 (H1, d, *J* = 5.9), 8.012 (H10, s), 7.53–6.65 (9H, ArH).

[Zn(L²)₂], 2. Yield: 84 mg (89%). Elemental Anal. Calcd. for C₃₂H₂₀Cl₂N₄O₂Zn: C, 64.77; H, 3.40; N, 9.44. Found: C, 64.92; H, 3.57; N, 9.68. IR (KBr, cm⁻¹): ν(C=N) 1630; ν(C–O_{phenoxo}) 1217. ¹H NMR {300 MHz, DMSO–d₆, δ (ppm), *J* (Hz)}: 9.09 (H1, d, *J* = 5.8), 8.23 (H10, s), 7.78–6.30 (8H, ArH).

[Zn(L³)₂], 3. Yield: 90 mg (86%). Elemental Anal. Calcd. for C₃₄H₂₆N₄O₂Zn: C, 69.45; H, 4.46; N, 9.53. Found: C, 69.52; H, 4.48; N, 9.60. IR (KBr, cm⁻¹): ν(C=N) 1627; ν(C–O_{phenoxo}) 1213. ¹H NMR {300 MHz, DMSO–d₆, δ (ppm), *J* (Hz)}: 8.79 (H1, d, *J* = 5.7), 8.11 (H10, s), 7.44–6.09 (8H, ArH), 2.31 (CH₃, s).

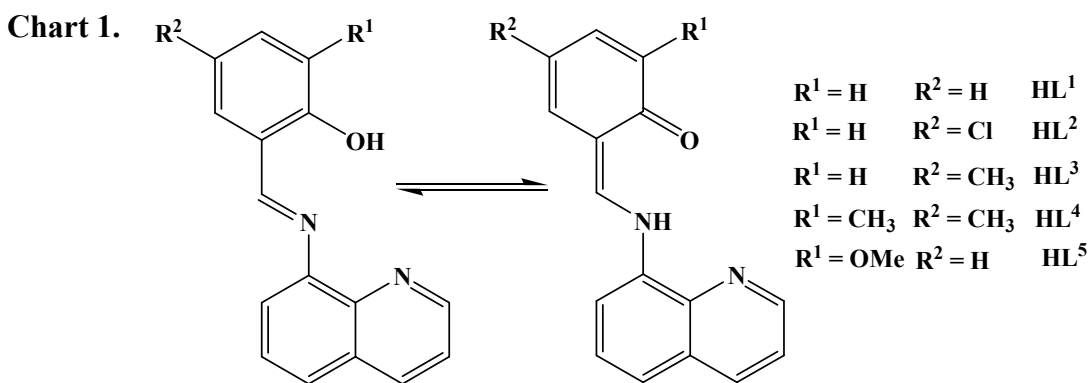
[Zn(L⁴)₂], 4. Yield: 75 mg (81%). Elemental Anal. Calcd. for C₃₆H₃₀N₄O₂Zn: C, 70.19; H, 4.91; N, 9.04. Found: C, 70.23; H, 4.92; N, 9.10. IR (KBr, cm⁻¹): ν(C=N) 1623; ν(C–O_{phenoxo}) 1220. ¹H NMR {300 MHz, DMSO–d₆, δ (ppm), *J* (Hz)}: 9.04 (H1, d, *J* = 5.7), 8.21 (H10, s), 7.71–6.97 (7H, ArH), 2.35 (CH₃, s), 2.32 (CH₃, s).

[Zn(L⁵)₂], 5. Yield: 72 mg (78%). Elemental Anal. Calcd. for C₃₄H₂₆N₄O₄Zn: C, 65.86; H, 4.23; N, 9.04. Found: C, 65.91; H, 4.25; N, 9.08. IR (KBr, cm⁻¹): ν(C=N) 1616; ν(C–O_{phenoxo}) 1225. ¹H NMR {300 MHz, DMSO–d₆, δ (ppm), *J* (Hz)}: 8.97 (H1, d, *J* = 5.9), 8.15 (H10, s), 7.57–6.89 (8H, ArH), 3.99 (OCH₃, s).

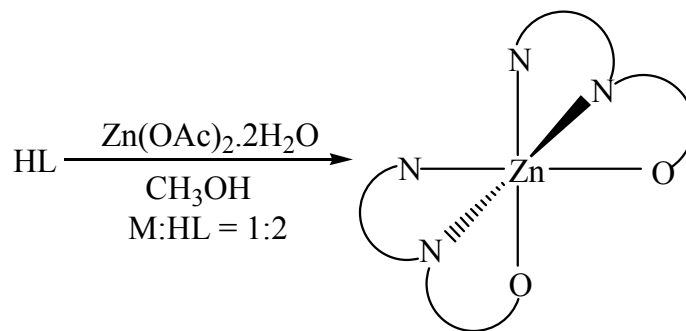
Results and discussion

Synthesis

Five tridentate ligands HL¹- HL⁵ (general abbreviation, HL) used in this work have been synthesized by reacting 8-aminoquinoline with the appropriate aldehyde in methanol are given in Chart 1. The ligands derived from 8-aminoquinoline and salicylaldehyde derivatives exist in the keto form in the solid state³⁶ however they exist both in the keto and enol form in solution.³⁷



The reaction of Zn(OAc)₂·2H₂O with HL in a ratio of 1:2 in methanol at room temperature in air affords orange colored complexes of composition [Zn(L)₂] in excellent yields. In the complex the ligands behave as a monoanionic *O*, *N*, *N* coordinating tridentate ligand. A schematic representation for the synthesis of complexes is given in Scheme 2.



Scheme 2 Schematic representation for the synthesis of the complexes

IR spectra of the complexes were recorded as KBr disks. In the complexes C–O_{phenoxo} stretches observed near 1213–1249 cm⁻¹ whereas the C=N stretch occurs as a

sharp peak in the frequency range 1616–1641 cm^{-1} . The complexes are diamagnetic and display well resolved ^1H NMR spectra in DMSO-d_6 solution. In complexes the azo methine proton was observed as a singlet near 8.20 ppm, and chemical shift at about 9.00 ppm is associated with the H atom adjacent to the pyridyl N atom of the coordinated ligands. The aromatic protons span in the range 7.80–6.30 ppm. The CH_3 groups are observed in the range 2.31–2.35 ppm whereas the OCH_3 signal occurs at 3.99 ppm. The details data for IR and NMR spectra are given in Experimental section.

Crystal Structure

The molecular structure of $[\text{Zn}(\text{L}^4)_2]$, **4** was determined by single-crystal X-ray diffractometry. The complex crystallizes in $P-1$ space group. The selected bond distances and angles for **4** are listed in Table 2, and the molecular view is shown in Fig. 1.

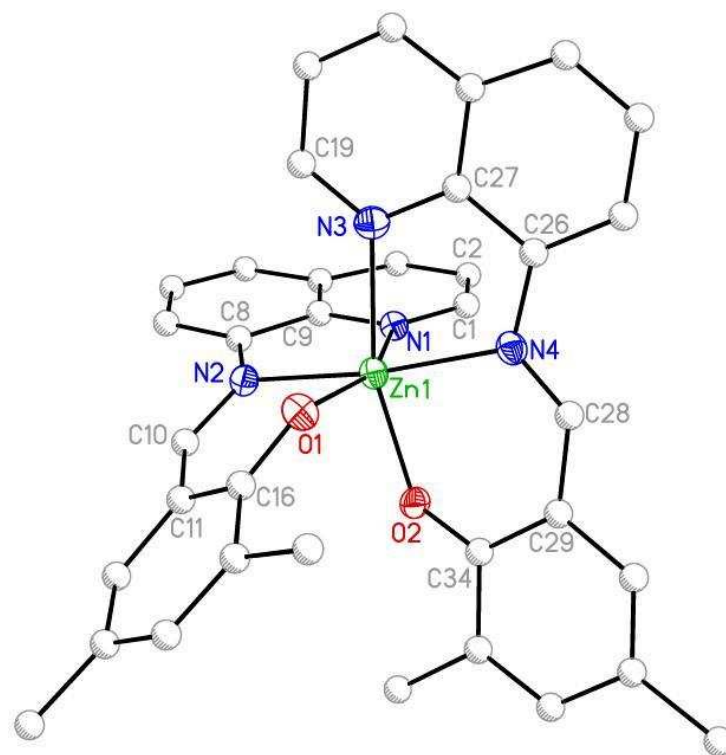


Fig. 1 ORTEP plot and atom labeling scheme of **4**. Hydrogen atoms have been omitted for clarity.

In complex **4** the ligand (HL⁴) acts as monoanionic *N, N, O* coordinating tridentate ligand and binds meridionally. Here the metal centre occupies a distorted octahedral geometry where the axial positions are occupied by one pyridyl nitrogen atom and phenoxo group and the equatorial positions are occupied by two imine and one pyridyl nitrogen atoms and one phenoxo group. In the complex, the Zn–O_{phenoxo} bond length is found to be 2.03 Å, while the Zn–N bond distances fall in the range 2.12–2.23 Å.

Table 2 Selected Bond Lengths (Å) and Angles (°) for **4**

Bond Lengths (Å)			
Zn1–N1	2.234(2)	Zn1–N4	2.125(2)
Zn1–N2	2.134(2)	Zn1–O1	2.047(2)
Zn1–N3	2.216(3)	Zn1–O2	2.034(2)
Bond Angles (°)			
N1–Zn1–N2	75.16(9)	N2–Zn1–O2	97.79(9)
N1–Zn1–N3	85.77(9)	N3–Zn1–N4	76.02(10)
N1–Zn1–N4	98.47(9)	N3–Zn1–O1	91.93(9)
N1–Zn1–O1	158.38(9)	N3–Zn1–O2	163.17(9)
N1–Zn1–O2	94.18(9)	N4–Zn1–O1	101.82(9)
N2–Zn1–N3	98.47(10)	N4–Zn1–O2	87.36(9)
N2–Zn1–N4	172.02(9)	O1–Zn1–O2	94.11(9)
N2–Zn1–O1	83.96(8)		

Geometry Optimization and Electronic Structure

The geometry optimizations of the ligands were performed in solution (THF) both in singlet ground state (S₀) and excited state (S₁) by DFT and TDDFT method respectively. The potential energy scan (Fig. 2) of HL¹ at S₀ state reveals that the keto (dihedral angle between two planes made by salicylaldehyde moiety and quinoline moiety is 0.4°) tautomeric form is more stable by an amount of energy 2.175 kcal mol⁻¹ than the corresponding nonplanar enol form (dihedral angle between two planes made

by salicylaldehyde moiety and quinoline moiety is 26.6°), which is consistent with the X-ray structure of this type of Schiff bases.³⁶

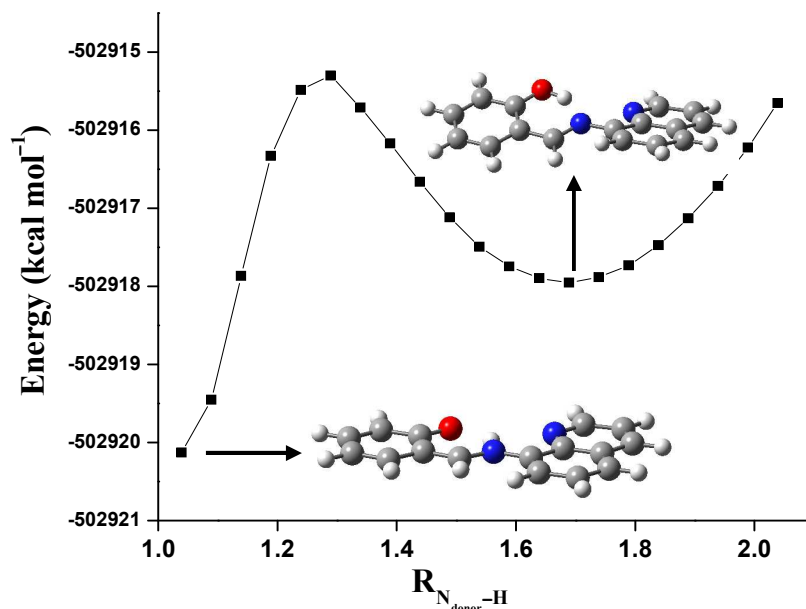


Fig. 2 Potential energy curve at ground S_0 state for HL^1 calculated at DFT/B3LYP level.

For the complexes we are able to optimize only the ground S_0 state geometries. Moreover we are unable to grow the single crystals suitable for structure determination for other systems. So the significant bond distances and angles of the optimized geometry of compound **4** along with one representative case **2** in their singlet ground S_0 state are compared with the crystal structure parameter of **4** (Table 3) The optimized structure for complex **2** and **4** are also shown in Fig. 3 as representative case.

Here the Zn(II) centre occupies a distorted octahedral geometry. The crystal structure data of **4** (Table 3) is in good agreement with optimized parameters and the slight discrepancy (maximum deviation 0.068 \AA for Zn1–N4 bond distance) comes from the crystal lattice distortion existing in real molecules. The optimized geometries of all the complexes do not show significant differences in the coordinate sphere around the metal center. It reveals that the ligands bind in a similar fashion in the complexes.

Table 3 Selected Optimized Geometrical Parameters of complexes **2** and **4** in the Ground (S_0) State at B3LYP Levels and Experimental Bond length (\AA) and Angle ($^\circ$) for complex **4**

	Solution phase		Experimental
	2	4	4
Zn1–N1	2.226	2.234	2.234
Zn1–N2	2.200	2.193	2.134
Zn1–N3	2.226	2.234	2.216
Zn1–N4	2.200	2.193	2.125
Zn1–O1	2.071	2.067	2.047
Zn1–O2	2.069	2.067	2.034
N1–Zn1–O1	161.490	161.043	158.38
N2–Zn1–N4	172.170	171.463	172.02
N3–Zn1–O2	161.526	161.024	163.17

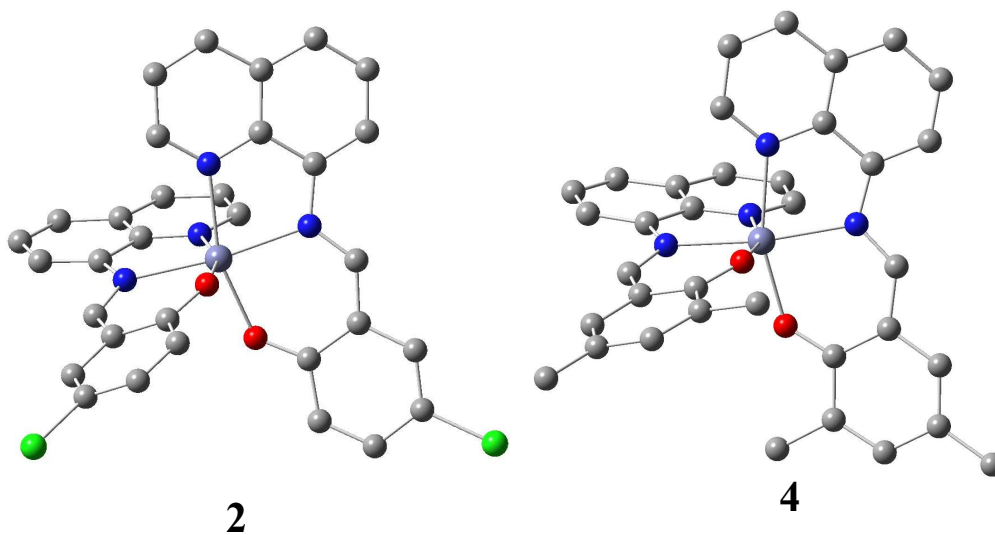


Fig. 3 Optimized molecular structures of **2** and **4**. (Zn: Pale violet, Cl: Green, N: Blue, O: Red, C: Grey. Hydrogen atoms are omitted for clarity)

The electron density at both HOMO and HOMO – 1 orbitals mainly reside on the salicylaldehyde moiety while the electron density at LUMO, LUMO + 1, LUMO + 2 and LUMO + 3, LUMO + 4 orbitals mainly reside on quinoline moiety. Similar pattern is observed for other complexes. The compositions of HOMO and LUMO are useful in

understanding the nature of transition as well as the absorption spectra of the complexes (*vide infra*).

Ligand Photophysical Study

The UV-vis absorption spectra of the ligands used in this present work were studied at room temperature in THF. All the ligands show two well resolved peaks in the region (450–473) and (337–360) nm. Fig. 4 shows experimental absorption spectra of all the ligands. The detailed spectral data are collected in Table 4.

The absorption energies associated with their oscillator strengths, the main configurations and their assignments calculated using TDDFT method using the S_0 geometry for HL² is discussed here and the related data are given in Table 5 whereas that for HL¹ is given in ESI (Table S1,†).

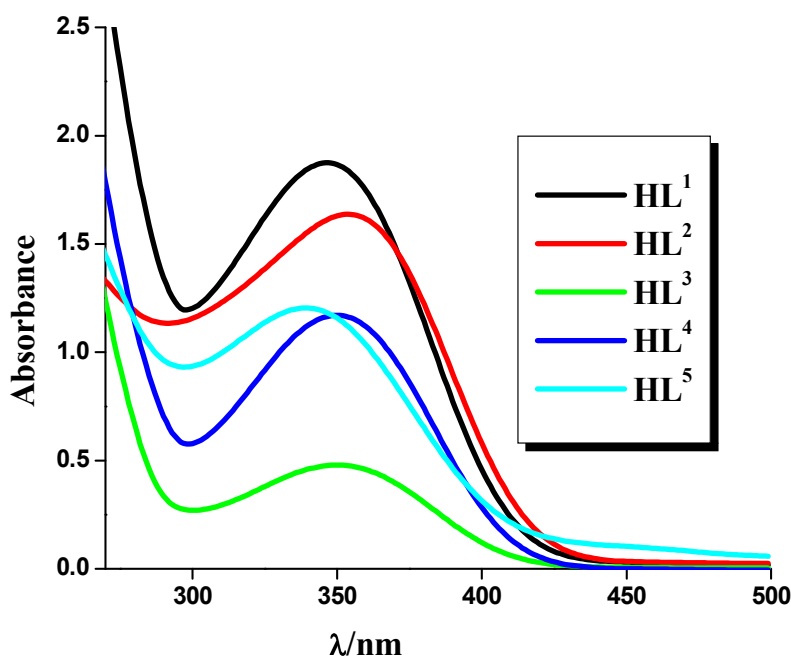


Fig. 4 Experimental UV-vis absorption spectra of all the ligands at room temperature in THF.

Table 4 Photophysical Parameters of the Ligands

Ligand	λ_{\max} , nm (ϵ , $M^{-1} \text{cm}^{-1}$)	λ_{emi} , nm	$\Delta\nu^a$ (nm)	Φ_F ($\times 10^{-3}$)
HL¹	468 (63)	533	65	1.42
	344 (10066)			
HL²	455 (149)	536	81	2.30
	360 (8690)			
HL³	450 (28)	523	73	1.60
	360 (2550)			
HL⁴	473 (247)	539	66	2.80
	351 (6162)			
HL⁵	454 (29)	557	103	3.80
	337 (6539)			

^a Stokes shifts.

Table 5 Selected Parameters for the Vertical Excitation (UV-vis Absorptions) and the Emission of HL²; Electronic Excitation Energies (eV) and Oscillator Strengths (f), Configurations of the Low-Lying Excited States of HL²; Calculation of the S₀–S₁ Energy Gaps Based on Optimized Ground-State Geometries (UV-vis Absorption) and the Optimized Excited-State Geometries (Fluorescence) (THF used as solvent)

Process	Electronic Transitions	Composition	Excitation energy	Oscillator strength (f)	CI	λ_{exp} (nm)
Absorption	S ₀ → S ₁	HOMO → LUMO	2.6388 eV (470 nm)	0.4180	0.70565	455
	S ₀ → S ₃	HOMO – 1 → LUMO HOMO → LUMO + 1	3.4097 eV (363 nm)	0.2564	0.59290 0.37802	360
Emission	S ₁ → S ₀	HOMO → LUMO	2.3087 eV (537 nm)	0.3229	0.70710	536

In case of the ligand HL² at ground state (S₀) HOMO is composed of 76 % of salicylaldehyde moiety and 24 % of the quinoline moiety while HOMO – 1 is composed of 36 % of salicylaldehyde moiety and 64 % of the quinoline moiety and HOMO – 1 is stabilized by 0.946 eV compared to HOMO. Similarly in LUMO the contribution of salicylaldehyde moiety (62 %) is greater than that of quinoline moiety whereas in LUMO + 1 the electron density is mainly residing at quinoline moiety (82 %). The energy difference between HOMO and LUMO is 3.504 eV. The calculated absorption bands are

located at 470 and 363 nm for HL² (Fig. 6), which are in good agreement with experimental results of 455 and 360 nm (Table 5). These two absorption bands can be assigned to the S₀ → S₁ and S₀ → S₃ transitions, respectively with ILCT character (Table 5). Similar calculations were carried out also for HL¹ and given in ESI (Fig. S1 and Table S1,†).

The fluorescence behavior of all the ligands discussed in this present work was studied at room temperature in THF solution (Fig. 5). All the ligands display red shifted emission spectra and their maxima occur in the range 530–560 nm with large Stokes shift (65–103 nm). In solution, at room temperature, all the ligands were weak emitters having low quantum yields (Φ_F) in the range (1.02–3.8) × 10⁻³. The luminescence parameters for all the ligands are listed in Table 4. The fluorescence intensity of HL¹ is much greater compared to other ligand system and this may be due to the incorporation of bulky group in case of other ligands the probability of intersystem crossing increases which reduces the fluorescence intensity for other ligand system compared to HL¹.

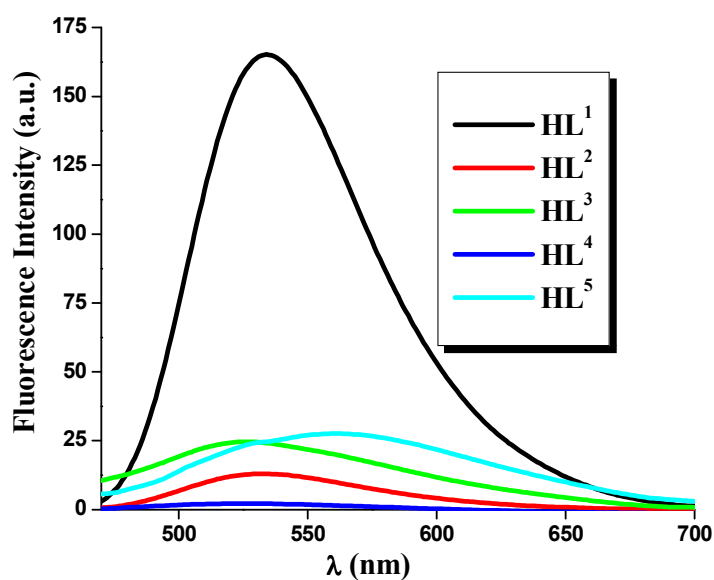


Fig. 5 Experimental Emission spectra of all the ligands at room temperature in THF.

In order to study the emission property, the excited state (S₁) geometry was optimized³⁸⁻³⁹ in THF solution by time-dependent DFT (TDDFT) method using CPCM for all the ligands. The energy gap between the S₀ and S₁ state, calculated with the

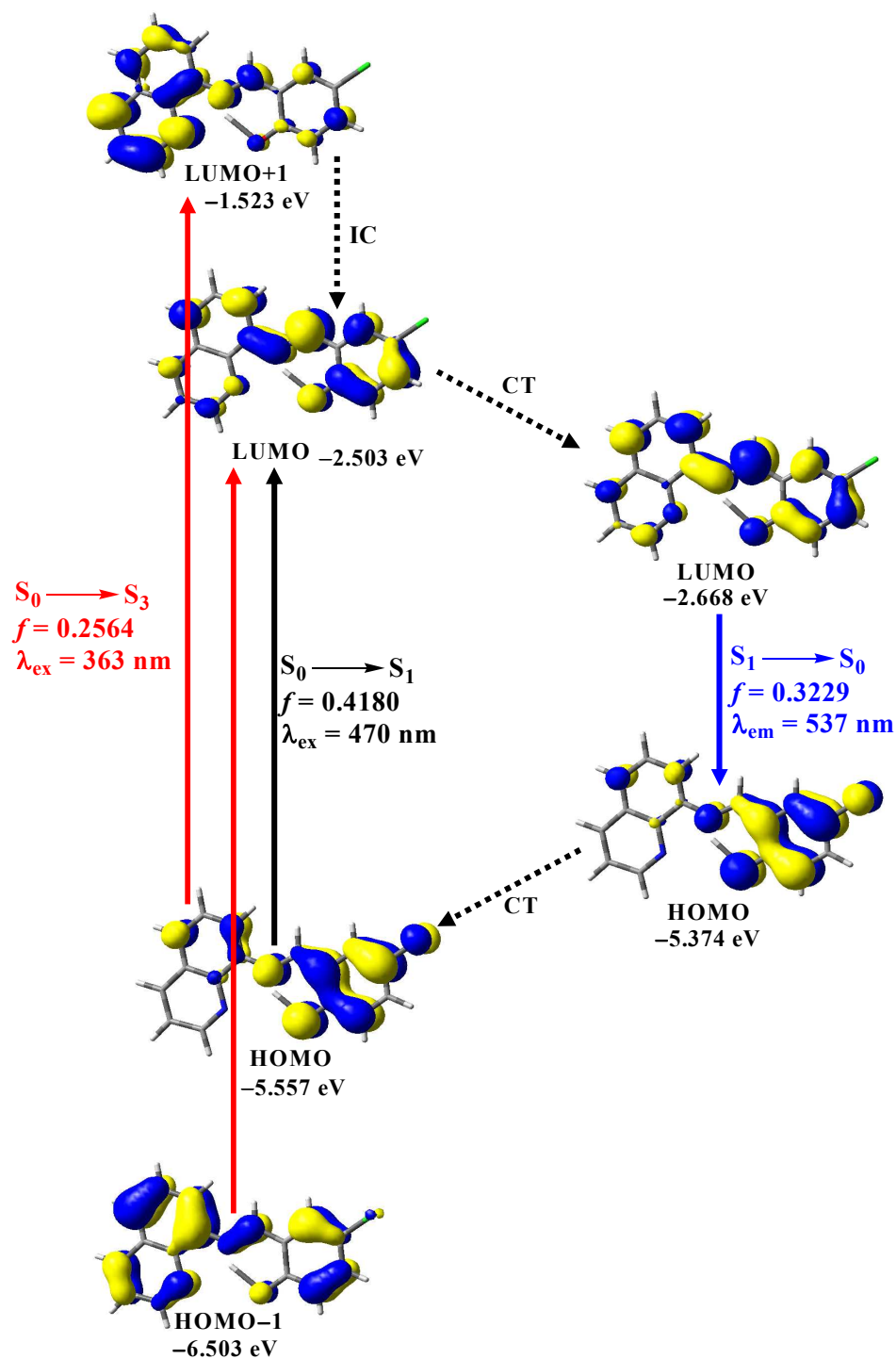


Fig. 6 Frontier molecular orbitals involved in the UV-vis absorption and emission of HL^2 . IC stands for internal conversion and CT stands for conformation transformation. Excitation and radiative decay process are marked as solid lines and the non-radiative processes are marked by dotted lines.

optimized S_1 state geometry, is the fluorescence emission wavelength.³⁸⁻³⁹ DFT study shows more coplanar structure at S_1 excited state compared to S_0 ground state for all the ligands. This geometry relaxation upon photoexcitation imparts remarkable effect on the energy level of the molecular orbitals. In case of HL^2 the LUMO is stabilized by 0.1657 eV at the S_1 state geometry compared to that at S_0 state geometry while the HOMO is destabilized by 0.1834 eV for S_1 state geometry compared to that at S_0 state geometry. As a result, the energy difference between the HOMO and LUMO is greatly decreased at the S_1 state compared to that at S_0 state geometry and this geometry relaxation is the main origin of large Stoke shift. The similar type of situation is observed for other ligands. For HL^2 the fluorescence wavelength was calculated as 537 nm (in THF) which is in very good agreement with the experimental value of 536 nm (Table 5). The calculated fluorescence spectral data for HL^1 is given in ESI as a representative case (Table S1,†).

Absorption Study of the Complexes

The mode of coordination of ligands ($HL^1 - HL^5$) with Zn^{2+} was investigated by absorption spectrophotometric titration at 25°C in THF solution. Fig. 7 describes a representative UV-vis titration curve of HL^2 with various concentration of Zn^{2+} ion. From Fig. 7, it has been observed that with increasing concentration of Zn^{2+} ion the absorption intensity of free ligand HL^2 at 360 nm gradually decreases with small blue shift and the absorption intensity at 455 nm gradually increases with an isosbestic point at 407 nm. It is to be noted that there is no changes of the absorption intensity both at 360 and 455 nm after the addition of excess of 0.5 equivalent of Zn^{2+} ion with respect to 1.0 equivalent of HL^2 . This result corroborates with the formation of 1:2 complex in solution. The same spectral behaviors are also documented for other ligands and the spectral changes for UV-vis titrations of other systems are given in ESI (Fig. S2 to S5,†).

Comparative experiments on Zn^{2+} -sensing characteristics with the ligands series were carried out with 0.1 mM HL solutions with the addition of 0.5 equivalent of Zn^{2+} . The experimental absorption spectra and the spectral parameters for all the complexes are given in Fig. 8 and Table 6. The isolated complexes exhibit similar spectral behaviour.

To get better insight to experimental absorption values TDDFT calculations were done for two complexes (**2** and **4**) on the basis of the optimized geometry. The calculated

absorption energies associated with their oscillator strengths, the main configurations and their assignments of **2** is given in Table 7 whereas that for complexes **4** is given in ESI (Table S2,†).

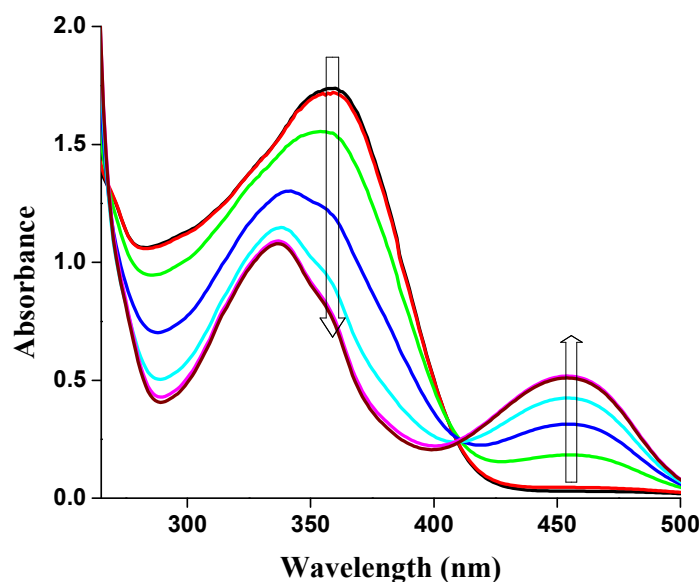


Fig. 7 Spectrophotometric titrations of HL² (0.1 mM) with various numbers of equivalent of Zn(ClO₄)₂·6H₂O in THF at room temperature ([Zn²⁺] = 0, 0.01, 0.02, 0.03, 0.04, 0.05 mM).

Table 6 Photophysical Parameters of the complexes

Complex	λ_{\max} , nm (ϵ , M ⁻¹ cm ⁻¹)	λ_{emi} , nm	$\Delta\nu^a$ (nm)	Φ_F
1	466 (781) 350 (10150)	540	74	0.3923
2	454 (2590) 374 (5455)	546	92	0.4409
3	450 (558) 350 (2472)	546	96	0.241
4	473 (533) 351 (6140)	571	98	0.0049
5	454 (990) 346 (4235)	572	118	0.0104

^a Stoke shift.

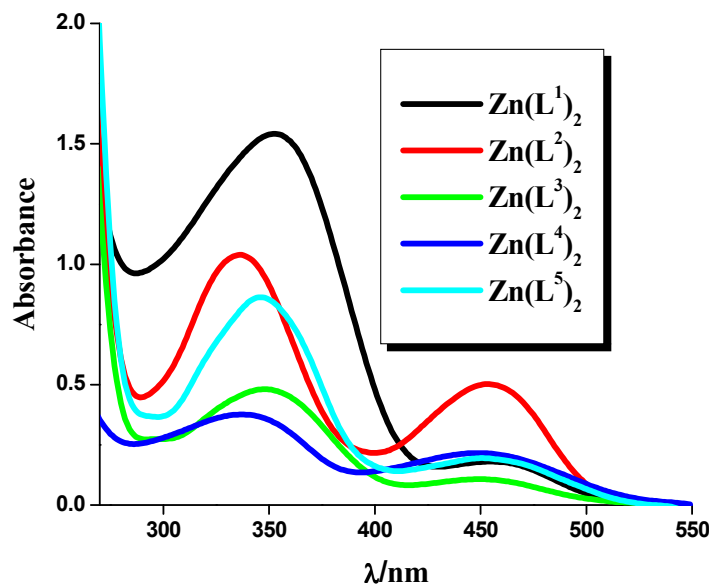


Fig. 8 Experimental UV-vis absorption spectra of all the complexes at room temperature in THF.

Table 7 Main calculated optical transition for complex 2 with composition in terms of molecular orbital contribution of the transition, Vertical excitation energies and Oscillator strength in THF

Excitation	Composition	Excitation energy	Oscillator strength (<i>f</i>)	CI	Assign	λ_{exp} (nm)
1	HOMO - 1 \rightarrow LUMO	2.6836 eV	0.3393	0.6253	ILCT	454
	HOMO \rightarrow LUMO + 1	(462 nm)		-0.3189	ILCT	
2	HOMO - 1 \rightarrow LUMO + 1	2.7100 eV	0.1852	0.6932	ILCT	
	HOMO \rightarrow LUMO	(457 nm)		-0.1171	ILCT	
3	HOMO - 1 \rightarrow LUMO + 2	3.2934 eV	0.0144	0.6759	ILCT	374
	HOMO \rightarrow LUMO + 3	(376 nm)		0.1760	ILCT	
4	HOMO - 5 \rightarrow LUMO	3.3726 eV	0.1286	-0.1428	ILCT	
	HOMO - 4 \rightarrow LUMO + 1	(368 nm)		-0.1574	ILCT	
	HOMO - 3 \rightarrow LUMO			-0.1578	ILCT	
	HOMO - 1 \rightarrow LUMO + 2			-0.1931	ILCT	
	HOMO \rightarrow LUMO + 3			0.6117	ILCT	

Here lowest lying distinguishable singlet \rightarrow singlet absorption band at 450 nm can be attributed to the HOMO - 1 \rightarrow LUMO, HOMO \rightarrow LUMO + 1, HOMO - 1 \rightarrow LUMO + 1 and HOMO \rightarrow LUMO transitions and these can be assigned to $\pi(\text{L}) \rightarrow \pi^*(\text{L})$

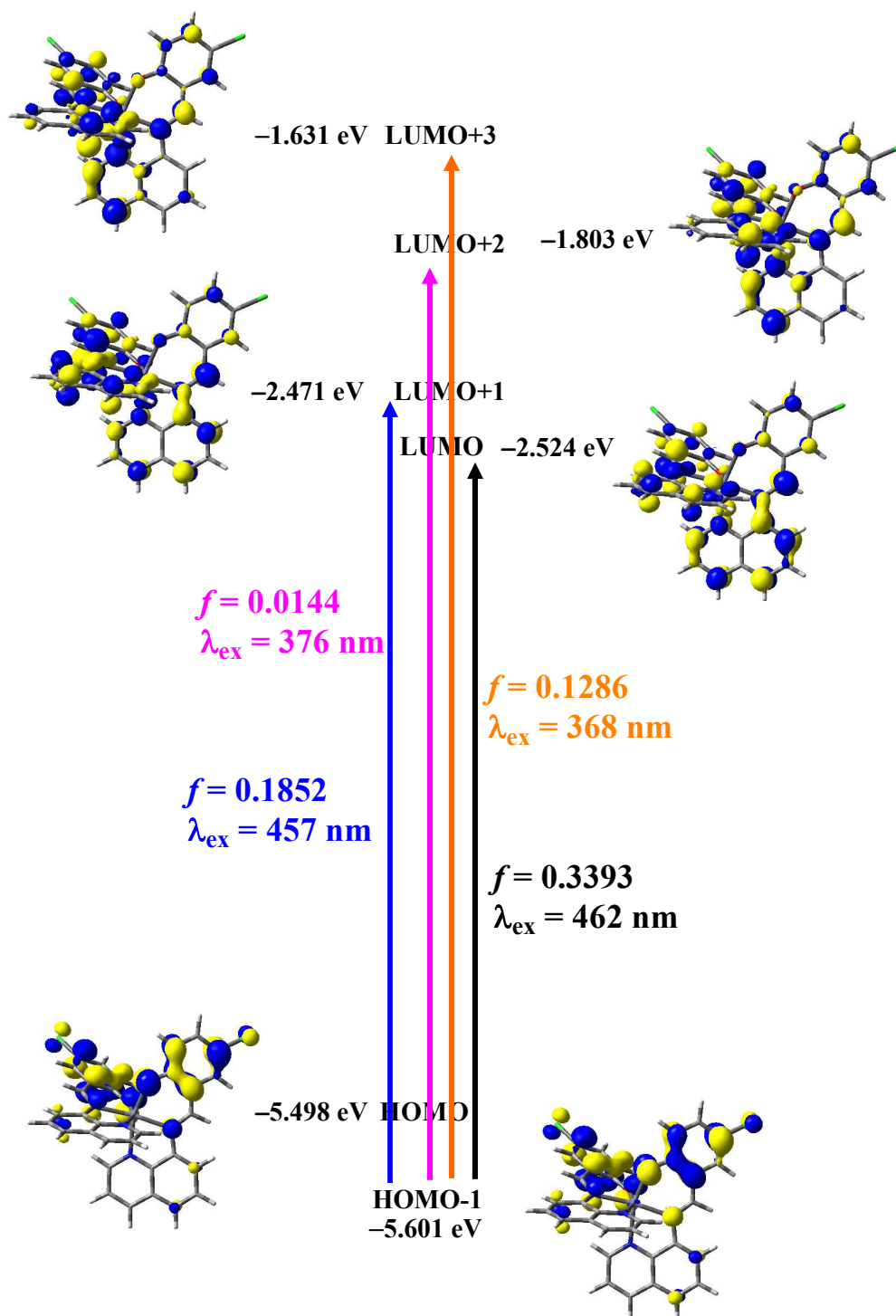


Fig. 9 Frontier molecular orbitals involved in the UV-vis absorption of complex 2.

transitions with ILCT character. The absorption band at 374 nm consists of more than one excitation. The excitations observed at energies are 3.2934 eV ($\lambda = 376 \text{ nm}$ and $f =$

0.0144) and 3.3726 eV ($\lambda = 368$ nm and $f = 0.1286$) and these are due to HOMO \rightarrow LUMO + 3, HOMO - 1 \rightarrow LUMO + 2, HOMO - 3 \rightarrow LUMO, HOMO - 4 \rightarrow LUMO + 1, HOMO - 5 \rightarrow LUMO transitions with ILCT character. Frontier molecular orbitals involved in the UV-vis absorption for complex **2** are given in Fig. 9. In summary, the TDDFT calculations reveal that the ICT process is occurring from salicylaldehyde moiety (donor) to quinoline moiety (acceptor).

Fluorescent Properties of Complexes

The coordination mode as well as binding constant of HL to Zn^{2+} ion was investigated by fluorescence titration in THF at room temperature. The ligands emit very weak fluorescence near 530 nm ($\lambda_{\text{ex}} = 450$ nm) with quantum yields span in the range $(1.02\text{--}3.8) \times 10^{-3}$ (Table 4). However the fluorescence intensity enhances remarkably with small bathochromic shift when excited at 450 nm upon addition of Zn^{2+} ions. The details luminescence parameters are listed in Table 6. The enhancement of quantum yields are 275, 190, 150, 1.75 and 2.75 fold for HL¹–HL⁵, respectively (Table 6). Fig. 10 illustrates the enhancement of emission intensity of HL² with the increase concentration of Zn^{2+} ions from 0 to 1.0 equivalent. Inset of Fig. 10 describes a plot of emission intensity at 546 nm against the titration of Zn^{2+} from 0 to 1.0 equivalent. It is clear from the plot that the fluorescence intensity reaches a plateau after addition of 0.5 equivalents of Zn^{2+} ions and there is no significant enhancement of the fluorescence intensity on further addition of Zn^{2+} . This result strongly corroborates with the formation of 1:2 complex between Zn^{2+} and HL². The titration curves of other ligands are given in ESI (Fig. S6 to S9,†).

In complex, the ligands bind as monoanionic form to the Zn^{2+} forming a six-membered and five-membered chelating ring with the ligands. TDDFT study reveals that the transition near 450 nm is mainly associated with the HOMO and LUMO. The electron density in HOMO is mainly localized on phenol ring while that in LUMO is localized on the quinoline ring, which results in complete ICT from the phenol ring (donor, HOMO) to quinoline ring (acceptor, LUMO) with the enhancement of fluorescence intensity via CHEF mechanism.

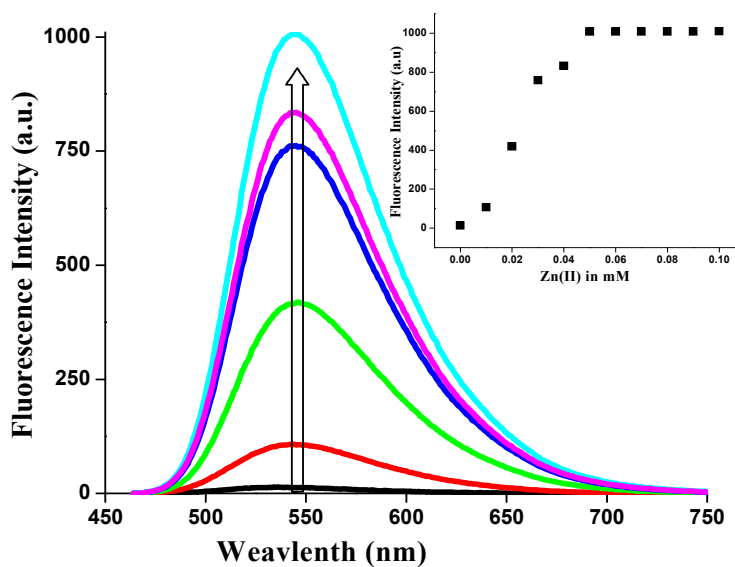


Fig. 10 Fluorescence emission spectra of HL² upon addition of Zn(II) in THF, $\lambda_{\text{ex}} = 454$ nm at room temperature ($[\text{HL}^2] = 0.1 \text{ mM}$, $[\text{Zn(II)}] = 0.01, 0.02, 0.03, 0.04$ and 0.05 mM). Inset: Fluorescence intensity vs different concentration of Zn(II) ion.

Table 8 Binding constant values for all complexes

Complex	Binding Constant ($\times 10^4$)
1	2.80
2	1.25
3	0.75
4	15.37
5	3.00

The binding constant values have been determined from the emission intensity data³⁸ using the modified Benesi-Hildebrand equation:

$$1 / \Delta F = 1 / \Delta F_{\text{max}} + (1 / K[\text{C}]) (1 / \Delta F_{\text{max}})$$

to establish the binding abilities of the ligands with Zn²⁺. Here, $\Delta F = F_x - F_0$ and $\Delta F_{\text{max}} = F_{\infty} - F_0$, where F_0 , F_x and F_{∞} are the emission intensities of the ligand used in the absence of Zn²⁺, at an intermediate Zn²⁺ concentration, and at a concentration of complete

interaction, respectively, and where K is the binding constant and $[C]$ the Zn^{2+} concentration. The binding constant values for the complexes are given in Table 8. The binding constants values reveal that the ligands have strong binding abilities to Zn^{2+} .

Comparative experiments on Zn^{2+} -sensing characteristics with the ligands series were carried out with 0.1 mM HL solutions with the addition of 0.5 equivalents Zn^{2+} and the corresponding emission spectra are shown in Fig. 11. The isolated complexes exhibit similar spectral behaviour. We found that the ligands HL^4 and HL^5 is a very weak and a moderate emitter, respectively in the presence of Zn^{2+} , where the other three ligands (HL^1 , HL^2 , HL^3) exhibit remarkable fluorescence enhancement after metal-ion complexation (Table 6).

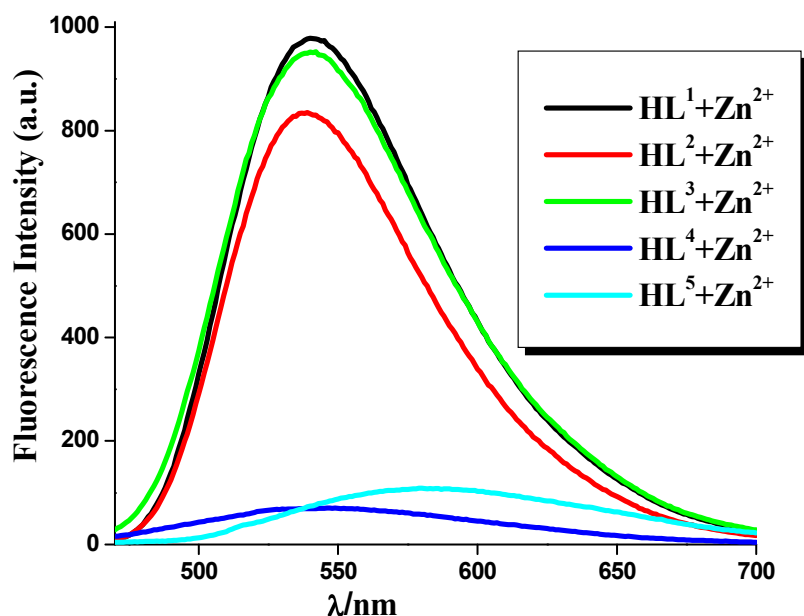


Fig. 11 Experimental Emission spectra of all the complexes at room temperature in THF.

It is interesting to note that the complexes which are associated with the ligands having bulky group (HL^4 and HL^5 , Chart 1) at the ortho position of the phenol group of salicylaldehyde moiety obviously caused the low quantum yields which may be attributed to the vibrational effects. Therefore it is believed that the effect of substitution on reducing the emission intensity may be attributed to the loss of conjugation or vibrational quenching due to steric effect originated from the bulky group at ortho position.

Metal ion competition Studies

We have studied the fluorescence intensity behavior upon addition of various metal ions. All the ligands in the present study behave similarly. The metal ion binding selectivity was assayed in 0.1 mM THF with excitation at 454 nm. Fig. 12 shows the fluorescence intensity of HL² in the presence of different metal ions. We observed that among the metal ions studied only Zn²⁺, Cd²⁺ metal ions change the emission behavior of HL² (Fig. 13). However, the enhancement of the fluorescence intensity in case of Zn(II) is much higher than that of Cd(II) ion.^{15,42} Other biogenic cations, such as Na⁺ and K⁺ in living cells, neither enhanced nor quenched the emission intensity, as shown in Fig. 13 and this can be attributed to the very weak complexing ability of alkali metal ions with the ligand. Other metal ions such that Ca²⁺, Ni²⁺, Co²⁺, Fe³⁺, Mn²⁺, and Cu²⁺ were quenched the emission intensity as there is a probability of an electron and energy transfer between the metal ion and ligands.

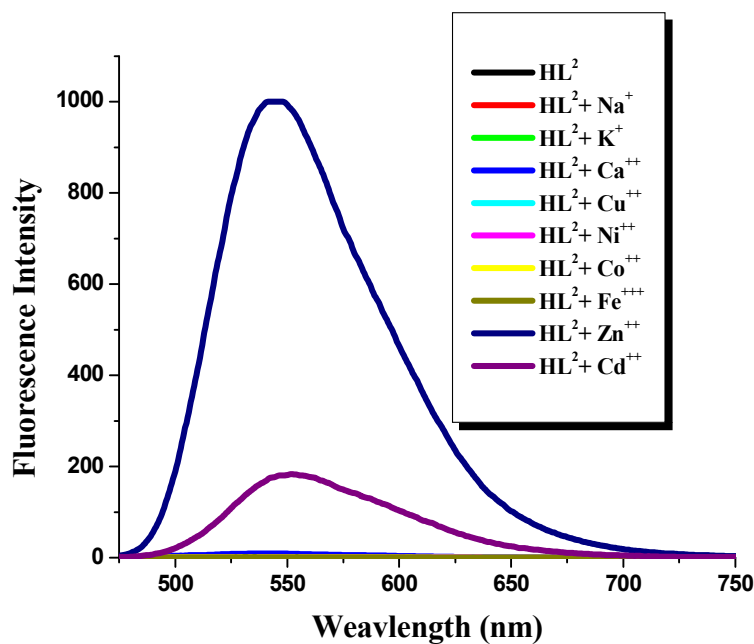


Fig. 12 Relative fluorescence intensity change of HL² in the presence of various metal ions at room temperature in THF, $\lambda_{\text{ex}} = 454$ nm.

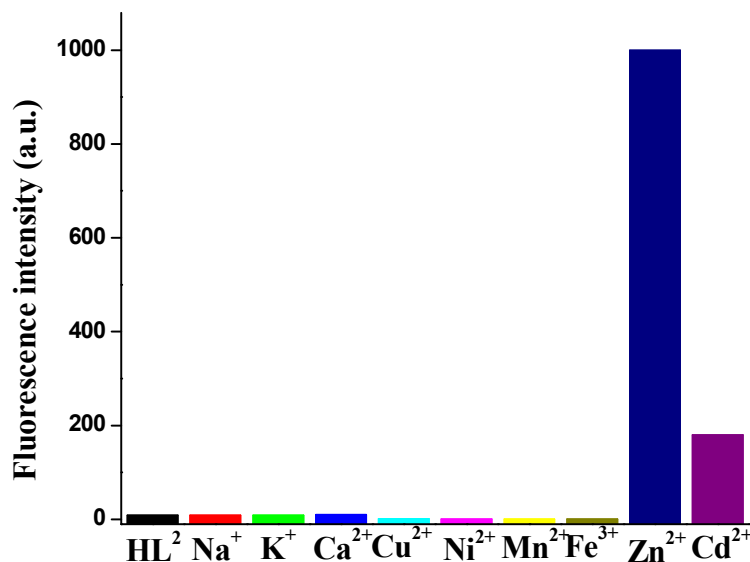


Fig. 13 Histogram plot of fluorescence intensity change of HL² in the presence of various metal ions at room temperature in THF, $\lambda_{\text{ex}} = 454$ nm.

Conclusion

In summary we have characterized five tridentate ligands having quinoline moiety and their binding behavior with Zn(II) metal ion. The geometry optimization of the ligands reveals that ligand stable in their keto tautomeric form in ground state. The photophysical properties of the ligands were calculated with TDDFT approach. Emission intensity of all the ligands are enhanced significantly through the complexation with Zn(II) metal ion and form 1:2 (M:L) complex which was confirmed by fluorescence titration as well as X-ray structure. Our study reveals that in complexes the quantum yield (Φ_F) decreases significantly when bulky group incorporated at the ortho-position with respect to the phenolic group of the ligand. The geometry of the complexes as well as their spectral behaviors was studied by DFT and TDDFT method.

Acknowledgements

Financial assistance received from the Council of Scientific and Industrial Research, New Delhi, India, Science & Engineering Research Board, New Delhi, India is gratefully acknowledged. We are also thankful to Department of Science and Technology, New Delhi, India for the data collection on the CCD facility setup (Jadavpur University) under DST-FIST program. We also acknowledge CAS, Department of Chemistry, Jadavpur University and DST-PURSE program for other facilities. Pallab Mondal and Amar Hens are also thankful to CSIR, New Delhi and UGC, New Delhi for the research fellowship. Authors are also thankful to Karan Goswami for preliminary work.

Notes

Inorganic Chemistry Section, Department of Chemistry, Jadavpur University, Kolkata, 700 032, India. E-mail: kajalrajak@hotmail.com // kkrajak@chemistry.jdvu.ac.in

† Electronic Supplementary Information (ESI) available: X-ray crystallographic file in CIF format for 4.CH₃OH; Figure S1-S9 and Table S1-S2. CCDC reference number 944740.

References

- (1) (a) Y. Wand, N. Herron, V. V. Grushin, D. D. LeCloux and V. A. Petrov, *Appl. Phys. Lett.*, 2001, **79**, 449-451; (b) H. Xin, F. Y. Li, M. Shi, Z. Q. Bian and H. C. Huang, *J. Am. Chem. Soc.*, 2003, **125**, 7166-7167; (c) A. Tsuboyama, H. Iwawaki, M. Furugori, T. Mukaide, J. Kamatani, S. Igawa, T. Moriyama and S. Miura, T. Takiguchi, S. Okada, M. Hoshino and K. Ueno, *J. Am. Chem. Soc.*, 2003, **125**, 12971-12979.
- (2) (a) Z. C. Wen and Y. B. Jiang, *Tetrahedron*, 2004, **60**, 11109-11115; (b) F. Y. Wu, Z. Li, L. Guo, X. Wang, M. H. Lin, Y. F. Zhao and Y. B. Jiang, *Org. Biomol. Chem.*, 2006, **4**, 624-630.
- (3) (a) V. Thiagarajan, P. Ramamurthy, D. Thirumalai and V. T. Ramakrishnan, *Org. Lett.*, 2005, **7**, 657-660; (b) T. Gunnlaugsson, H. D. P. Ali, M. Glynn, P. E.

- Kruger, G. M. Hussey, F. M. Pfeffer, C. M. G. dos Santos and J. Tierney, *J. Fluoresc.*, 2005, **15**, 287-299.
- (4) S. S. Sun, J. A. Anspach, A. J. Lees and P. Y. Zavalij, *Organometallics*, 2002, **21**, 685-693.
- (5) (a) V. Luxami and S. Kumar, *RSC Advances*, 2012, **2**, 8734-8740; (b) S. Park, J. E. Kwon and S. Y. Park, *Phys. Chem. Chem. Phys.*, 2012, **14**, 8878-8884.
- (6) T. Harano, K. Kikuchi, Y. Urano and T. Nagano, *J. Am. Chem. Soc.*, 2002, **124**, 6555-6562.
- (7) S. C. Burdette and S. J. Lippard, *Coord. Chem. Rev.*, 2001, **216**, 333-361.
- (8) S. C. Burdette and S. J. Lippard, *Proc. Natl. Acad. Sci. U.S.A.*, 2003, **100**, 3605-3610.
- (9) M. D. Shultz, D. A. Pearce and B. Imperiali, *J. Am. Chem. Soc.*, 2003, **125**, 10591-10597.
- (10) G. K. Walkup, S. C. Burdette, S. J. Lippard and R. Y. Tsien, *J. Am. Chem. Soc.*, 2000, **122**, 5644-5645.
- (11) S. C. Burdette, G. K. Walkup, B. Springler, R. Y. Tsien and S. J. Lippard, *J. Am. Chem. Soc.*, 2001, **123**, 7831-7841.
- (12) C. R. Goldsmith and S. J. Lippard, *Inorg. Chem.*, 2006, **45**, 555-561.
- (13) Y. Mikata, M. Wakamatsu, A. Kawamura, N. Yamanaka, S. Yano, A. Odani, K. Morihiro and S. Tamotsu, *Inorg. Chem.*, 2006, **45**, 9262-9268.
- (14) Y. Mikata, M. Wakamatsu and S. Yano, *Dalton Trans.*, 2005, **0**, 545-550.
- (15) C. Bazzicalupi, A. Bencini, E. Berni, A. Bianchi, P. Fornasari, C. Giorgi and B. Valtancoli, *Eur. J. Inorg. Chem.*, 2003, 1974-1983.
- (16) (a) A. Sarkar, A. K. Ghosh, V. Bertolasi and D. Ray, *Dalton Trans.*, 2012, **41**, 1889-1896; (b) L. J. Daumann, K. E. Dalle, G. Schenk, R. P. McGeary, P. V. Bernhardt, D. L. Ollis and L. R. Gahan, *Dalton Trans.*, 2012, **41**, 1695-1708; (c) Z. Xu, J. Yoon and D. R. Spring, *Chem. Soc. Rev.*, 2010, **39**, 1996-2006.
- (17) (a) G. Masanta, C. S. Lim, H. J. Kim, J. H. Han, H. M. Kim and B. R. Cho, *J. Am. Chem. Soc.*, 2011, **133**, 5698-5700; (b) H. -Y. Lin, P. -Y. Cheng, C. -F. Wan and A. -T. Wu, *Analyst*, 2012, **137**, 4415-4417; (c) Y. Mikata, A. Yamashita, A.

- Kawamura, H. Konno, Y. Miyamoto and S. Tamotsu, *Dalton Trans.*, 2009, **0**, 3800-3806.
- (18) (a) Y. Zhang, X. Guo, L. Jia, S. Xu, Z. Xu, L. Zheng and X. Qian, *Dalton Trans.*, 2012, **41**, 11776-11782; (b) G. Consiglio, S. Failla, P. Finocchiaro, I. P. Oliveri and S. D. Bella, *Dalton Trans.*, 2012, **41**, 387-395; (c) G. Consiglio, S. Failla, P. Finocchiaro, I. P. Oliveri and S. D. Bella, *Inorg. Chem.*, 2010, **49**, 5134-5142.
- (19) (a) E. T. Elsaesser, H. J. Bakker, H. J. *Ultrafast Hydrogen Bonding Dynamics and Proton Transfer Processes in the Condensed Phase*, Kluwer, Dordrecht, 2002. (b) X. Zhou, B. Yu, Y. Guo, X. Tang, H. Zhang and W. Liu, *Inorg. Chem.*, 2010, **49**, 4002-4007; (c) B. Zhang, K. Cao and X. Zeng, *Eur. J. Inorg Chem.*, 2012, 3844-3851.
- (20) (a) M. Irie, *Chem. Rev.*, 2000, **100**, 1683-1684; (b) R. Pandey, P. Kumar, A. K. Singh, M. Shahid, P. Li, S. K. Singh, Q. Xu, A. Misra and D. S. Pandey, *Inorg. Chem.*, 2011, **50**, 3189-3197; (c) S. A. Ingale and F. Seela, *J. Org. Chem.*, 2012, **77**, 9352-9356.
- (21) S. M. Aldoschin, L. O. Atovmian, *Problemy Kristalokhimii*, Poraj-Koshic, M. Eds., Nauka, Moscow, 1984.
- (22) P. Fita, E. Luzina, T. Dziembowska, D. Kopeć, P. Piątkowski, Cz. Radzewicz and A. Grabowska, *Chem. Phys. Lett.*, 2005, **416**, 305-310.
- (23) W. H. Melhuish, *J. Phys. Chem.*, 1961, **65**, 229-235.
- (24) P. Mondal, A. Hens, S. Basak and K. K. Rajak, *Dalton Trans.*, 2013, **42**, 1536-1549.
- (25) E. Runge and E. K.U. Gross, *Phys. Rev. Lett.*, 1984, **52**, 997-1000.
- (26) (a) M. E. Casida, C. Jamoroski, K. C. Casida and D. R. Salahub, *J. Chem. Phys.*, 1998, **108**, 4439-4449; (b) R. E. Stratmann, G. E. Scuseria and M. J. Frisch, *J. Chem. Phys.*, 1998, **109**, 8218-8224; (c) R. Bauernschmitt and R. Ahlrichs, *Chem. Phys. Lett.*, 1996, **256**, 454-464.
- (27) (a) A. D. Becke, *J. Chem. Phys.*, 1993, **98**, 5648-5652; (b) C. Lee, W. Yang and R. G. Parr, *Phys. Rev. B*, 1988, **37**, 785-789.

- (28) (a) M. Cossi, N. Rega, G. Scalmani and V. Barone, *J. Comput. Chem.*, 2003, **24**, 669-681; (b) M. Cossi and V. Barone, *J. Chem. Phys.*, 2001, **115**, 4708-4717; (c) V. Barone and M. Cossi, *J. Phys. Chem. A*, 1998, **102**, 1995-2001.
- (29) (a) A. Douhal, F. Lahmani and A. Zewail, *Chem. Phys.*, 1996, **207**, 477-498 ; (b) J. Catalan and J. L. P. de Paz, *J. Phys. Chem. A*, 2001, **105**, 7315-7316.
- (30) P. J. Hay and W. R. Wadt, *J. Chem. Phys.*, 1985, **82**, 299-310.
- (31) M. J. Frisch, G. W. Trucks, H. B. Schlegel, G. E. Scuseria, M. A. Robb, J. R. Cheeseman, G. Scalmani, V. Barone, B. Mennucci, G. A. Petersson, H. Nakatsuji, M. Caricato, X. Li, H. P. Hratchian, A. F. Izmaylov, J. Bloino, G. Zheng, J. L. Sonnenberg, M. Hada, M. Ehara, K. Toyota, R. Fukuda, J. Hasegawa, M. Ishida, T. Nakajima, Y. Honda, O. Kitao, H. Nakai, T. Vreven, J. A. Montgomery Jr., J. E. Peralta, F. Ogliaro, M. Bearpark, J. J. Heyd, E. Brothers, K. N. Kudin, V. N. Staroverov, R. Kobayashi, J. Normand, K. Raghavachari, A. Rendell, J. C. Burant, S. S. Iyengar, J. Tomasi, M. Cossi, N. Rega, J. M. Millam, M. Klene, J. E. Knox, J. B. Cross, V. Bakken, C. Adamo, J. Jaramillo, R. Gomperts, R. E. Stratmann, O. Yazyev, A. J. Austin, R. Cammi, C. Pomelli, J. W. Ochterski, R. L. Martin, K. Morokuma, V. G. Zakrzewski, G. A. Voth, P. Salvador, J. J. Dannenberg, S. Dapprich, A. D. Daniels, Ö. Farkas, J. B. Foresman, J. V. Ortiz, J. Cioslowski and D. J. Fox, *Gaussian 09, (Revision A.1)*, Gaussian, Inc., Wallingford, CT, 2009.
- (32) N. M. O'Boyle, A. L. Tenderholt and K. M. Langner, *J. Comp. Chem.*, 2008, **29**, 839-845.
- (33) *SMART; SAINT; SADABS; XPREP; SHELXTL*; Bruker AXS Inc.: Madison, WI, 1998.
- (34) G. M. Sheldrick, v. *SHELXTL*, 6.14; Bruker AXS Inc.: Madison, WI, 2003.
- (35) C. K. Johnson, *ORTEP Report ORNL-5138*; Oak Ridge National Laboratory: Oak Ridge, TN, 1976.
- (36) T. Shibahara, M. Takahashi, A. Maekawa and H. Takagi, *Acta Cryst.*, 2010, **E66**, o429.
- (37) (a) F. Tisato, F. Refosco, A. Moresco, G. Bandoli, U. Mazzi and M. Nicolini, *J. Chem. Soc., Dalton Trans.*, 1990, 2225-2232; (b) T. Dziembowska, A.

- Rozwadowski and P. E. Hansen, *Magn. Reson. Chem.*, 2001, **39**, S67-S80; (c) B. Djukic, P. A. Dube, F. Razavi, T. Seda, H. A. Jenkins, J. F. Britten and M. T. Lemaire, *Inorg. Chem.*, 2009, **48**, 699-707; (d) H. Xu, Z. P. Ni, X. M. Ren and Q. J. Meng, *J. Mol. Struct.*, 2005, **752**, 153-157; (e) A. M. Donia and H. A. El-Boraey, *Transition Met. Chem.*, 1993, **18**, 315-318.
- (38) (a) J. R. Lakowicz, *Principles of Fluorescence Spectroscopy*, 2nd ed.; Kluwer Academic: New York, 1999; (b) B. Valeur, *Molecular Fluorescence: Principles and Applications*; Wiley-VCH Verlag: Weinheim, 2001.
- (39) N. J. Turro, V. Ramamurthya and J. C. Scaiano, *Principles of Molecular Photochemistry: An Introduction*, University Science Books: Sausalito, 2009.
- (40) (a) C. L. Dollberg and C. Turro, *Inorg. Chem.*, 2001, **40**, 2484-2485; (b) D. M. Roundhill, *Photochemistry and Photophysics of Metal Complexes*, J. P. Fackler, ed.; Modern Inorganic Chemistry Series, Plenum Press, New York, 1994.
- (41) (a) A. Mallick and Chahattopadhyay, *Photochem. Photobiol.*, 2005, **81**, 419-424; (b) H. A. Benesi and J. H. Hildebrand, *J. Am. Chem. Soc.*, 1949, **71**, 2703-2707; (c) N. J. Turro, *Modern Molecular Photochemistry*, Benjamin Cummings Publishing Co., Inc., Menlo Park, CA, 1978.
- (42) C. Bazzicalupi, A. Bencini, A. Bianchi, C. Giorgi, V. Fusi, B. Valtancoli, M. A. Bernado and F. Pina, *Inorg. Chem.*, 1999, **38**, 3806-3813.

Graphical Abstract for the contents

Synthesis, structure and spectral properties of *O, N, N* coordinating ligands and their neutral Zn(II) complexes: a combined experimental and theoretical study

Amar Hens, Pallab Mondal, and Kajal Krishna Rajak*

Five *O, N, N* coordinating ligands and their neutral Zn(II) complexes of general formula [Zn(L)₂] have been synthesized. The ligands and complexes are isolated and characterized by different spectroscopic techniques. X-ray structure of a representative complex has been determined. The electronic structure and photophysical properties of the ligands were calculated by DFT and TDDFT method. The binding constant of the ligands and the sensing property of Zn(II) with the ligands are studied. The fluorescence behavior of the ligands with other metal ions is given. The DFT calculation reveals that ICT process is responsible for enhancement of fluorescence intensity of ligands after complexation.

